Oncogenic transformation of diverse gastrointestinal tissues in primary organoid culture

Xingnan Li, Lincoln Nadauld, Akifumi Ootani, David C. Corney, Reetesh K. Pai, Olivier Gevaert, Michael A. Cantrell, Paul G. Rack, James T. Neal, Carol W-M. Chan, Trevor Yeung, Xue Gong, Jenny Yuan, Julie Wilhelmy, Sylvie Robine, Laura D. Attardi, Sylvia K. Plevritis', Kenneth E. Hung, Chang-Zheng Chen, Hanlee P. Ji, Calvin J. Kuo

Supplementary Information

Including

Supplementary Figures 1-11

Supplementary Discussion

Supplementary Figure 1

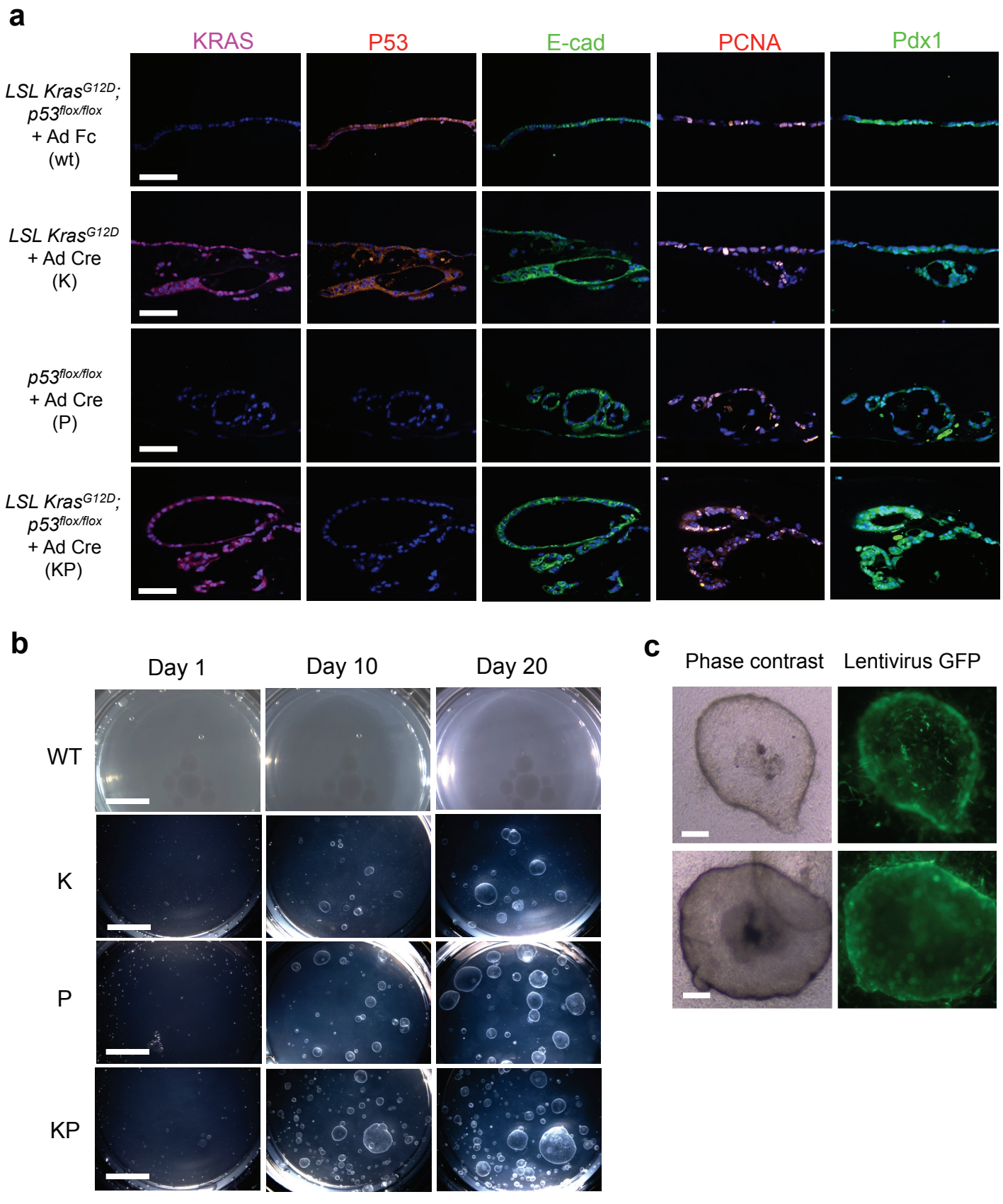

Supplementary Figure 1. Confirmation of loxP-Cre manipulation and epithelial dysplasia in LSL $Kras^{G12D}$; $p53^{flox/flox}$ neonatal pancreatic organoids .

(a) $Kras^{G12D}$ expression (Kras) and/or p53 deletion (p53) were confirmed by anti-Kras and/or anti-p53 immunofluorescence. Anti-E-cadherin (E-cadherin) immunofluorescence outlined the epithelial layer of dysplastic regions. Anti-PCNA (PCNA) immunofluorescence indicated hyperproliferative cells. Anti-Pdx1 immunofluorescence documented ductal cells in pancreatic organoids. Culture day 30, scale bars, 100 μm.

(b) Efficient passage of primary pancreatic organoids. Pancreatic organoid cultures were generated from neonatal mice harboring homozygous *Trp53* floxed (P) and/or *LSL* $Kras^{G12D}$ (K) alleles or both (KP) and subsequently infected with CreGFP-expressing adenovirus. On day 20, the organoids were dissociated and replated in a collagen matrix with air-liquid interface. Pictures were taken at day 1, 10 and 20 post-passage. scale bars, 5 mm.

(c) Efficient viral infection of passaged primary pancreatic organoids. Pancreatic organoid cultures were generated from the pancreas of neonatal mice harboring *Trp53* floxed (P) alleles ($p53^{flox/flox}$). At day 20, organoids underwent secondary passage and simultaneous infection with GFP-expressing lentivirus or retrovirus. Phase contrast (left) and GFP expressing (right) organoids were imaged after 7 additional days post-infection. scale bar, 200 μm.

Supplementary Figure 2

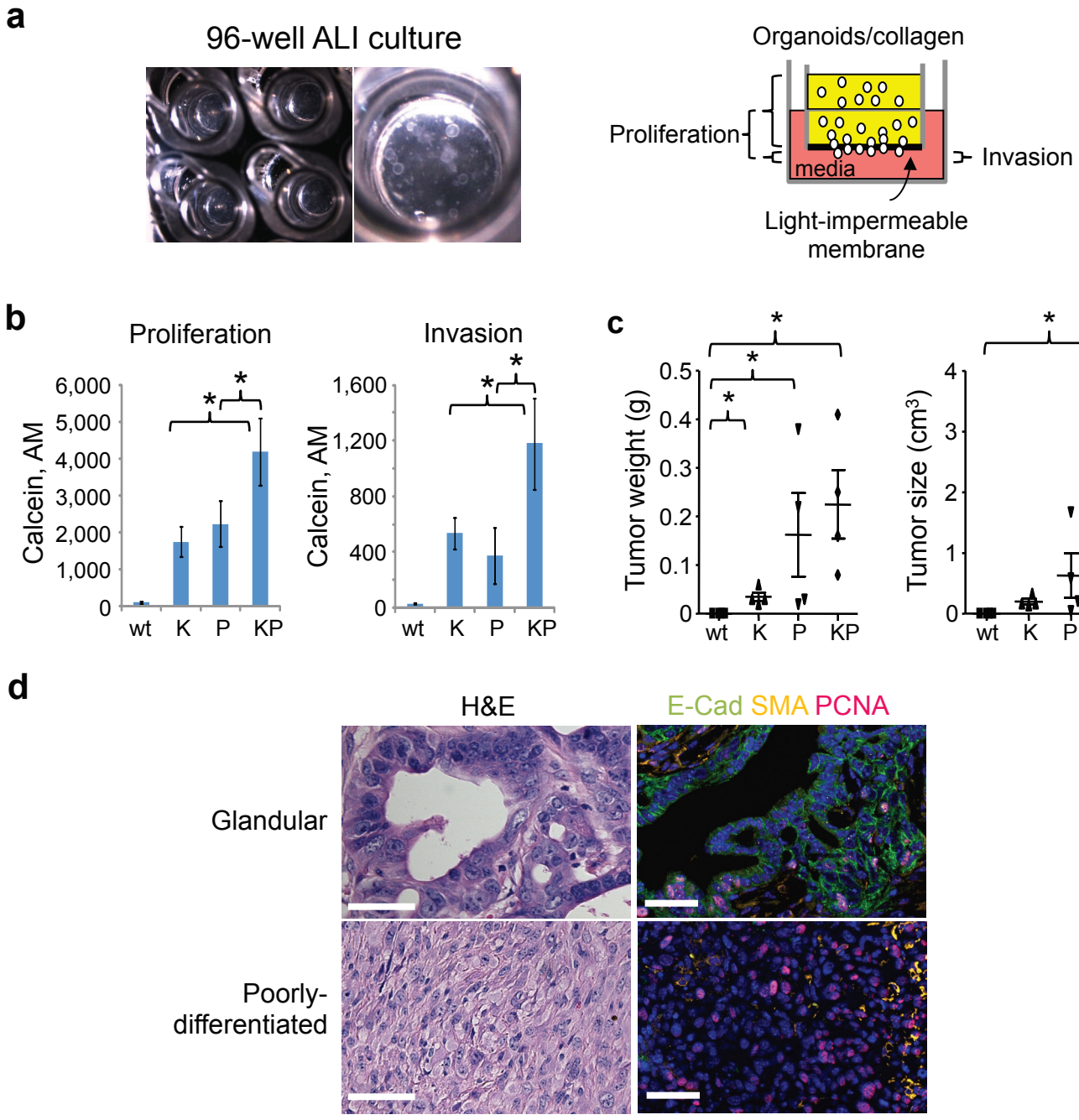

Supplementary Figure 2. ***In vitro*** **evaluation of pancreatic organoid proliferation and invasion and in vivo evaluation of organoid-derived pancreatic tumors.**

(a) 96-well organoid proliferation/invasion assay. Schematic of organoid growth in 96-well ALI culture, d14 after secondary plating with enlargement of a single well, demonstrating robust formation of secondary organoids. A light-impermeable transwell membrane allows tandem determination of proliferation vs. invasion.

(b) FACS-sorted EpCAM^{+} disaggregated cells from day 14 organoids of the indicated genotypes were replated at 10,000 cells/well into 96-well ALI culture to form secondary organoids. Wild-type organoids did not passage but after After 14 days of additional culture, proliferation and invasion in WT, K, P and KP organoids was determined by Calcein Red-Orange, AM fluorescence signal. n=12 wells/genotype, mean+/-SE. * = $P < 0.05$ for KP vs. K or P.

(c) Pancreatic tumor weight and size, day 30 after s.c. implantation of dissociated organoids of the indicated genotypes into NOD.Cg-Prkd^{cscid} Il2rg$^{tm1Sug/JicTac}$ mice, n=4 tumors/genotype. *= $P<0.05$.

(d) E-cadherin loss in poorly-differentiated areas of organoid-derived pancreatic tumors. H&E and immunofluorescence of glandular versus non-glandular areas of a KP tumor is depicted, d30 after organoid implantation. Scale bars, 50μm.

Supplementary Figure 3

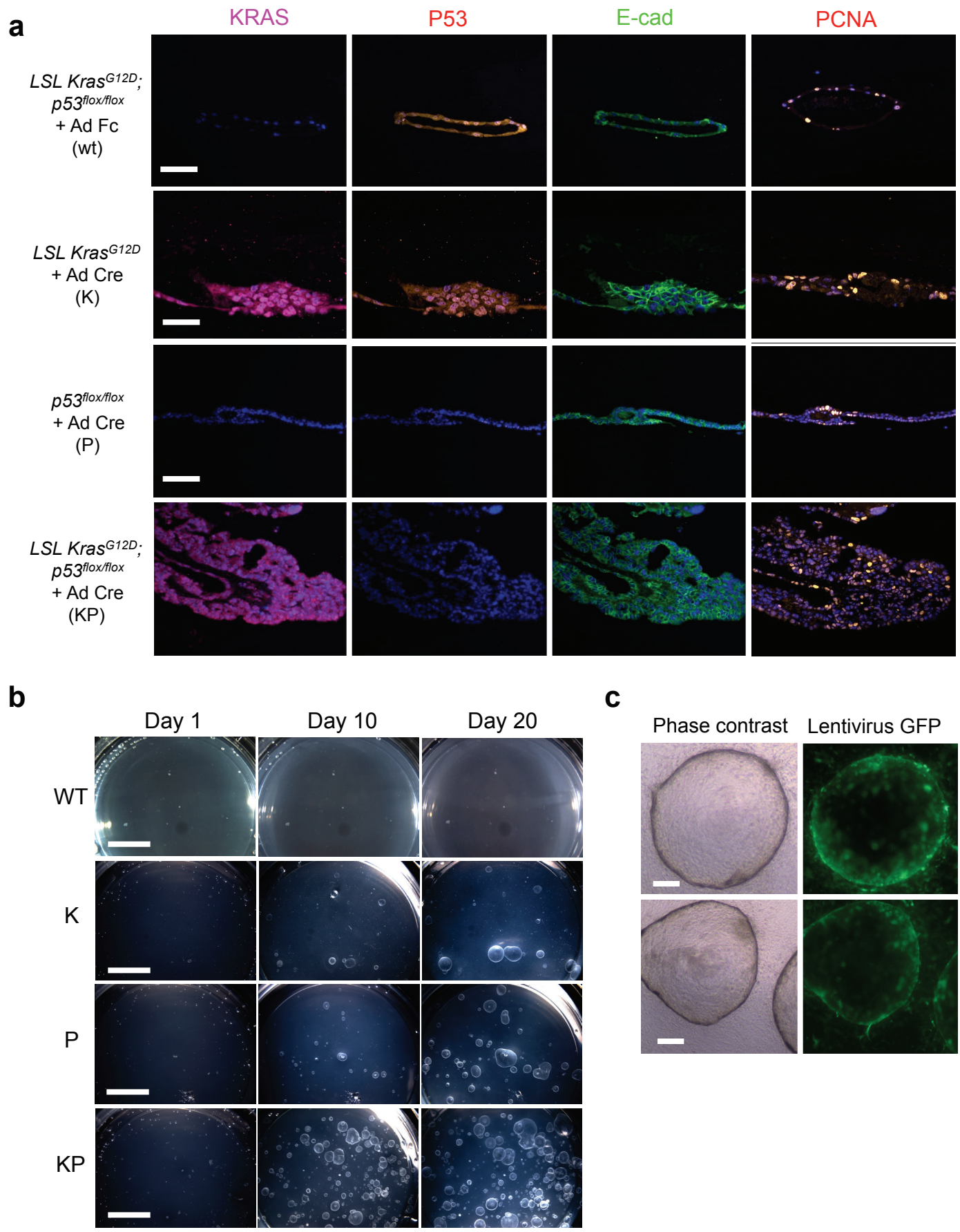

Supplementary Figure 3. Confirmation of loxP-Cre manipulation and epithelial dysplasia in LSL Kras^{G12D}; p53$^{flox/flox}$ gastric organoids.

(a) Kras^{G12D} expression (Kras) and/or p53 deletion (p53) were confirmed by anti-Kras and/or anti-p53 immunofluorescence staining. Anti-E-cadherin (E-cadherin) immunofluorescence staining confirmed the epithelial nature of dysplastic regions. Anti-PCNA immunofluorescence staining indicated hyperproliferative cells. Culture d30, scale bars, 100 µm.

(b) Gastric organoid cultures were made from the stomach of neonatal mice harboring *Trp53* floxed (P) (p53$^{flox/flox}$) and/or *LSL Kras^{G12D}* (K) alleles and subsequently infected with CreGFP-expressing adenovirus. On day 20, the organoids were dissociated and replated in a collagen matrix with air-liquid interface. Pictures were taken at day 1, 10 and 20 post-passage. scale bars, 5 mm.

(c) Gastric organoid cultures were generated from the stomach of neonatal mice harboring *Trp53* floxed (P) alleles (p53$^{flox/flox}$). At day 20, organoids underwent secondary passage and simultaneous infection with GFP-expressing lentivirus or retrovirus. Phase contrast (left) and GFP expressing (right) organoids were imaged after 7 additional days post-infection. scale bars, 200 µm.

Supplementary Figure 4

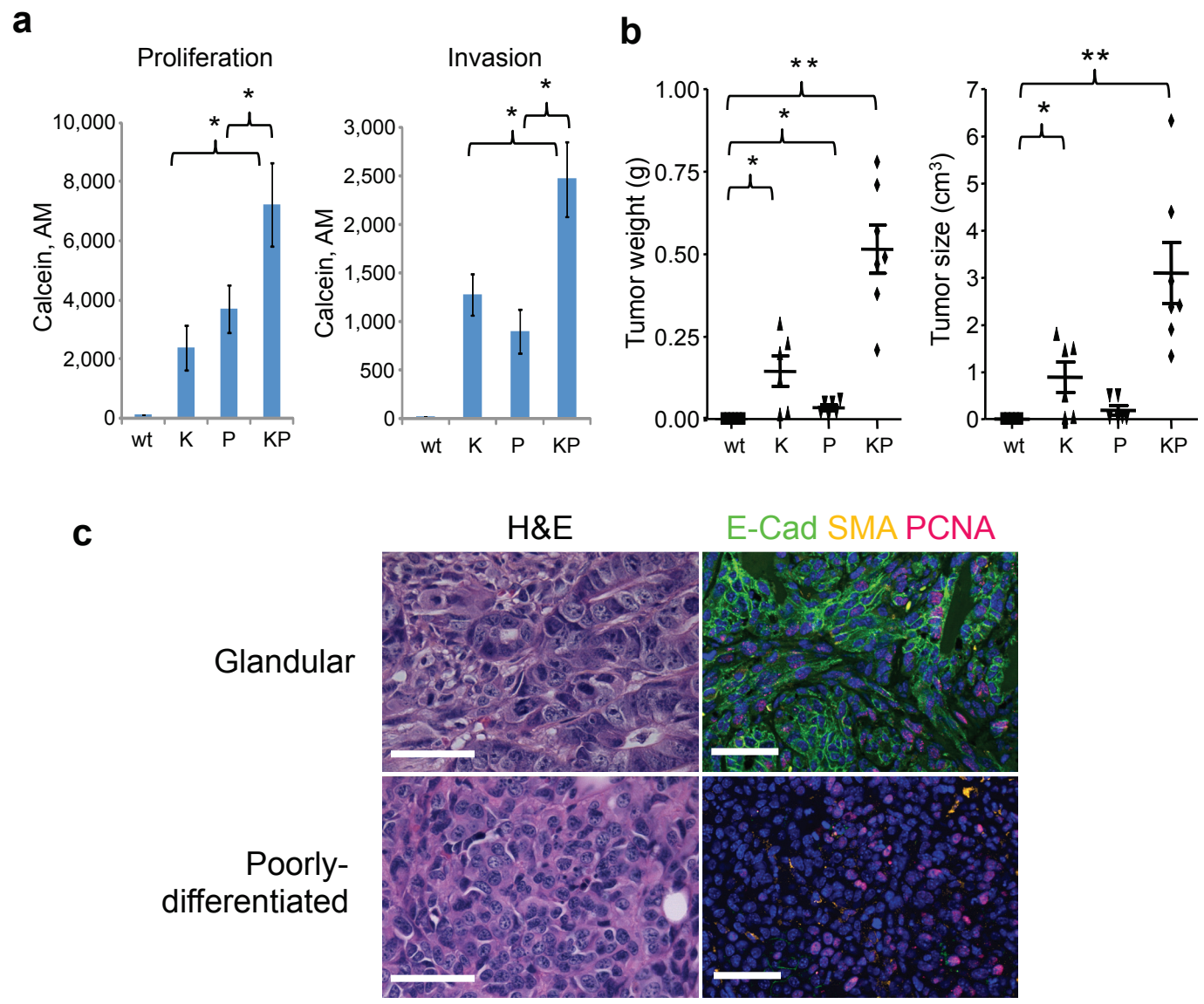

Supplementary Figure 4. 96-well gastric organoid proliferation and invasion assay.

(a) FACS-sorted EpCAM^{+} disaggregated cells from day 14 organoids of the indicated genotypes were replated at 10,000 cells/well into 96-well air-liquid interface culture to form secondary organoids. Wild-type organoids did not passage but after 14 days of additional culture, proliferation and invasion in WT, K, P and KP organoids was determined by Calcein Red-Orange, AM fluorescence signal. n=12 wells/genotype, mean+/-SE. * = $P < 0.05$ for KP vs. K or P.

(b) Tumor weight (left) and size (right), day 30 after s.c. implantation of dissociated organoids of the indicated genotypes into NOD.Cg-Prkd^{cscid} Il2rg$^{tm1Sug/JicTac}$ mice, n ≥ 6 tumors/genotype . ** = $P < 0.003$, *= $P<0.05$.

(c) H&E and immunofluorescence of glandular versus non-glandular areas of a KP tumor is depicted, d30 after organoid implantation. Scale bar, 50 μm.

Supplementary Figure 5

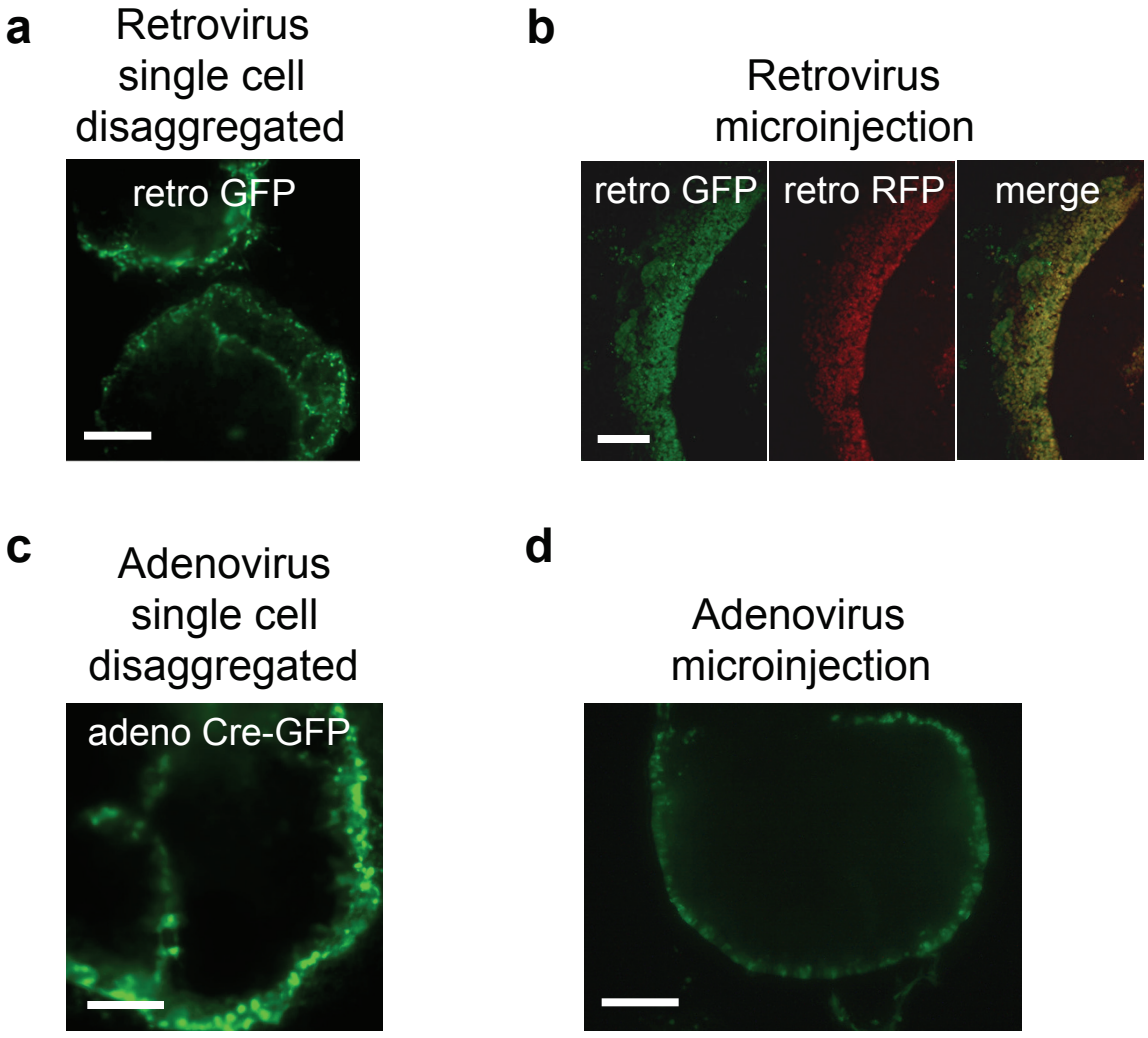

Supplementary Figure 5. Robust viral transduction of primary intestinal organoids by various methods.

(a) Retrovirus GFP transduction (LMP) by infection of disaggregated single-cell suspensions of Apc-null cells from tamoxifen-treated *Apc*$^{flox/flox}$*; villin-CreER* organoids. Live cell inverted fluorescence microscopy is depicted d14 after infection.
(b) Alternative method of retrovirus transduction (LMP) by microinjection of virus into the lumen of intact *Apc*-null intestinal organoids, d10 after infection. Robust coinfection of retrovirus GFP and RFP is shown by fluorescence microscopy of intrinsic GFP/RFP after whole mount fixation and embedding.
(c, d). Adenoviral infection of freshly disaggregated *Apc*-null organoids followed by seconday organoid formation (c) versus microinjection of adenovirus into the lumen of pre-formed organoids (d). d14 after infection is depicted.

All scale bars are 100 μm.

Supplementary Figure 6

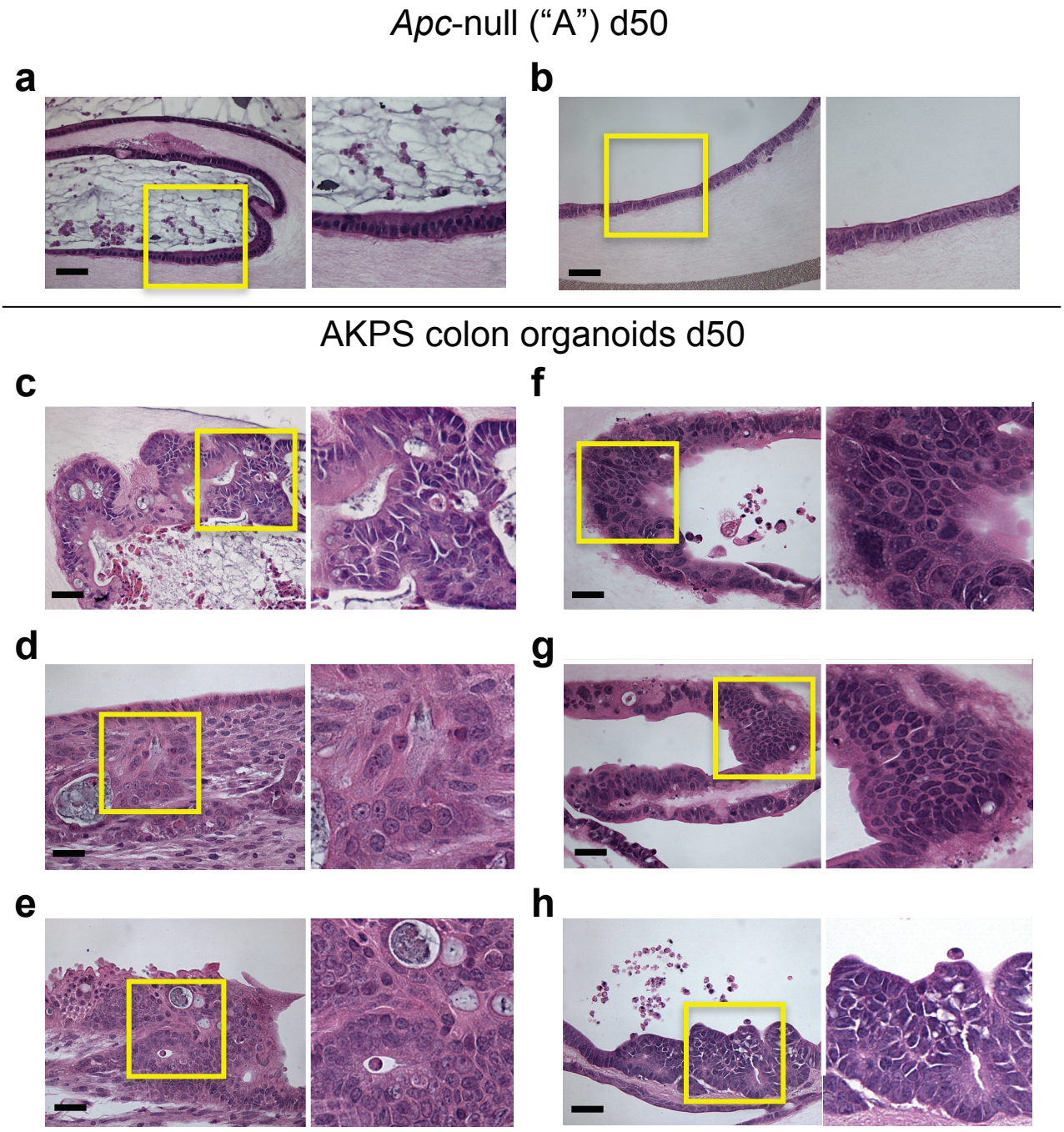

Supplementary Figure 6. Additional views of *Apc*-null ("A") versus AKPS colon organoids.
(a, b). *Apc*-null 1-gene organoids reproduced for comparison from **Figure 3**.
(c-h) AKPS 4-gene colon organoids. All images are culture day 50 after retroviral infection. (**c-e)** represent additional views of AKPS organoids from Figure 3e.
(**f-h)** represent additional examples of AKPS colon organoids. The yellow boxes are further enlarged in the adjacent panels. Note marked nuclear atypia, pleiomorphism and prominent nucleoli in AKPS but not *Apc*-null organoids. (d, e) represent adenocarcinoma with invasion. High grade dysplasia is present in c, f and g, with moderate dysplasia in h.

All scale bars are 50 μm.

Supplementary Figure 7

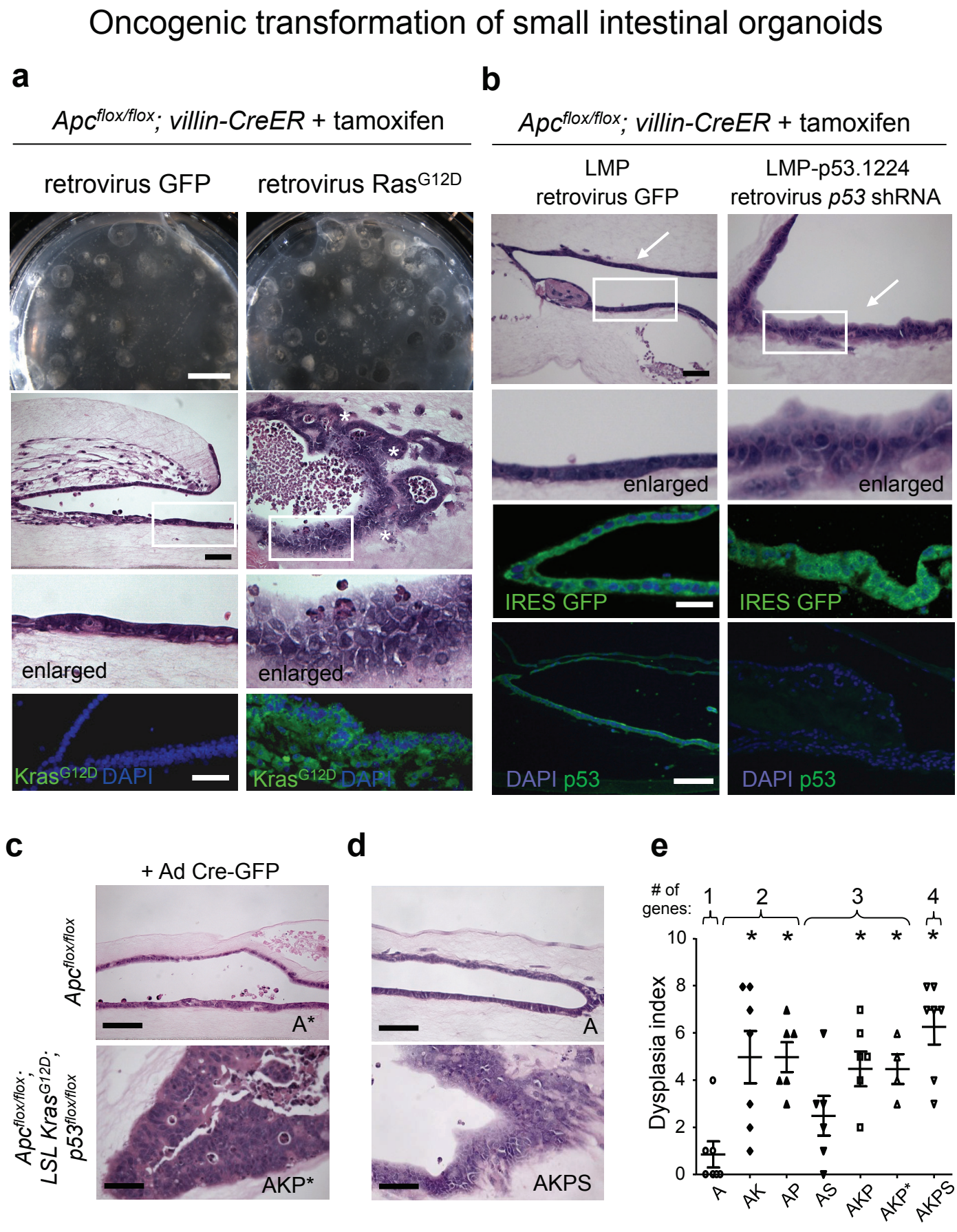

Supplementary Figure 7. Systematic evaluation of oncogene modules of increasing complexity in primary small organoids.

(a) Primary small intestinal organoids from adult *Apc$^{flox/flox}$; villin-CreER* mice were treated with tamoxifen to effect Apc deletion, followed by infection with retrovirus *Kras^{G12D}* (pBabe-puro *Kras^{G12D}*) or LMP-p53.1224 retrovirus (*p53* shRNA IRES GFP) or control retrovirus GFP (LMP) and culture for an additional 20 days.
top, *Kras^{G12D}* did not induce gross differences in growth of Apc-null organoids. Light stereomicroscope images are shown. Scale bar, 5 mm.
Middle, retrovirus *Kras^{G12D}* infection induced marked morphologic dysplasia with nuclear pleiomorphism and atypia, as well as a stratified epithelial layer. *= areas of robust invasion into the surrounding collagen. Scale bar, 50 μm.
Bottom, Anti-Kras IF. Endogenous Kras expression is low and the signal in h. predominantly represents Kras^{G12D}. Scale bar, 50 μm.

(b) Primary small intestinal organoids from adult *Apc$^{flox/flox}$; villin-CreER* mice were treated with tamoxifen to effect Apc deletion, followed by infection with retrovirus *Kras^{G12D}* (pBabe-puro *Kras^{G12D}*) or LMP-p53.1224 retrovirus (*p53* shRNA IRES GFP) or control retrovirus GFP (LMP) and culture for an additional 20 days (conditions identical to a, above)
Top, *p53* shRNA elicits high grade dysplasia with nuclear pleiomorphism, atypia, and stratification H&E staining, scale bar, 50 μm.
Middle, Anti-GFP immunofluorescence signal indicates robust infection from the IRES GFP cassette present in both the control and *p53* shRNA retroviruses, scale bar, 50 μm.
Bottom, Anti-p53 immunofluorescence indicates p53 knockdown, scale bar, 100 μm.

(c) Explanted tissue from *Apc$^{flox/flox}$; LSL Kras^{G12D}; p53$^{flox/flox}$* adult mice or *Apc$^{flox/flox}$* control mice was infected with Ad Cre-GFP at the time of plating. Organoid growth proceeded for 50 days followed by H&E staining of paraffin-embedded sections. High grade dysplasia and marked proliferation is observed in the 3-gene *Apc/Kras/p53* oncogene module (AKP*) versus the 1-gene *Apc* (A*) control. The "*" designation indicates that the AKP mutations were purely encoded by floxed mouse alleles and retroviral infection was not used. Scale bar, 50 μm.

(d) 4-gene module AKPS induced invasive adenocarcinoma histology in small intestine organoids. H&E, day 20.) Primary small intestinal organoids from adult *Apc$^{flox/flox}$; villin-CreER* mice were treated with tamoxifen to effect Apc deletion, followed by infection with retrovirus *Kras^{G12D}* (pBabe-puro *Kras^{G12D}*), LMP-p53.1224 retrovirus (*p53* shRNA IRES GFP) and retrovirus Smad4 shRNA (AKPS module) or control retrovirus GFP alone (A module). Scale bar, 50 μm.

(e) Dysplasia index for small intestine organoids, analyzed at day 20 post-retroviral infection, except for AKP* (day 50 post-Ad Cre-GFP). Each individual data point represents n=4-6 microscopic fields containing viable organoids. Mean +/- SE. * = $P < 0.01$ versus A.

Supplementary Figure 8

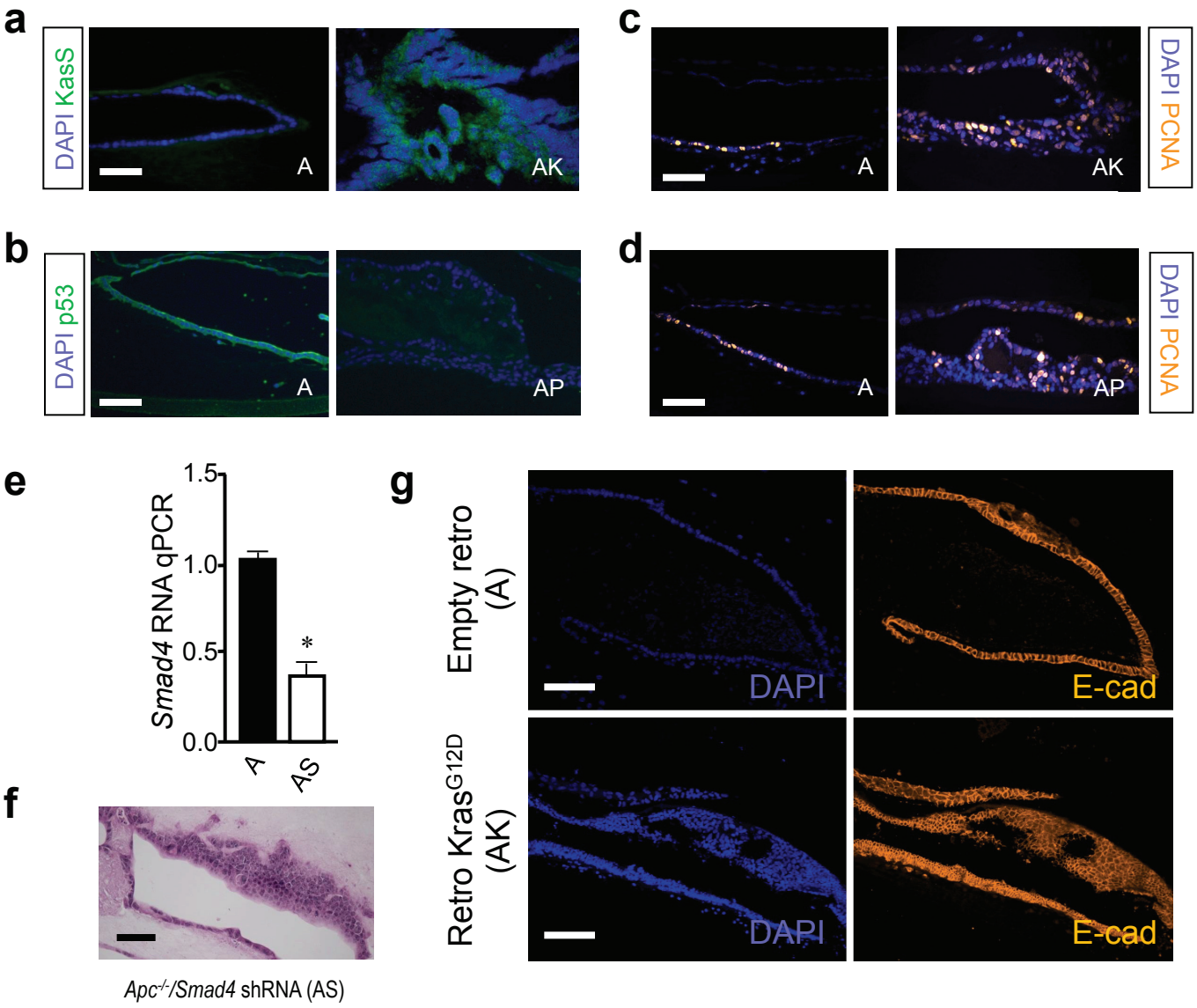

Supplementary Figure 8. Confirmation of oncogene manipulation and epithelial dysplasia in *Apc*-null small intestinal organoids.

(a, b). **(a)** *Kras*^{G12D} overexpression and **(b)** p53 knockdown confirmed by anti-Kras or anti-p53 immunofluorescence, d 20.
(c, d). PCNA staining of small intestinal organoids with and without *Kras*^{G12D} overexpression **(c)** or *p53* shRNA knockdown **(d)**.
(e) *Smad4* knockdown documented by qRT-PCR of FACS-sorted EpCAM^{+} GFP^{+} epithelium from tamoxifen-treated *Apc*$^{flox/flox}$*; villin-CreER* small intestine organoids infected with retrovirus *Smad4* shRNA/GFP (LMP backbone, AS) or LMP alone (A). n=3, Mean +/- SE. *= $P < 0.05$.
(f) H&E, d20 from Smad4 knockdown as in **(e)**.
(g) Anti-E-cadherin immunofluorescence confirms epithelial dysplasia in tamoxifen-treated small intestine *Apc*$^{flox/flox}$*; villin-CreER* organoids infected with retro *KRAS*^{G12D} (AK) or control retro (A).

Supplementary Figure 9

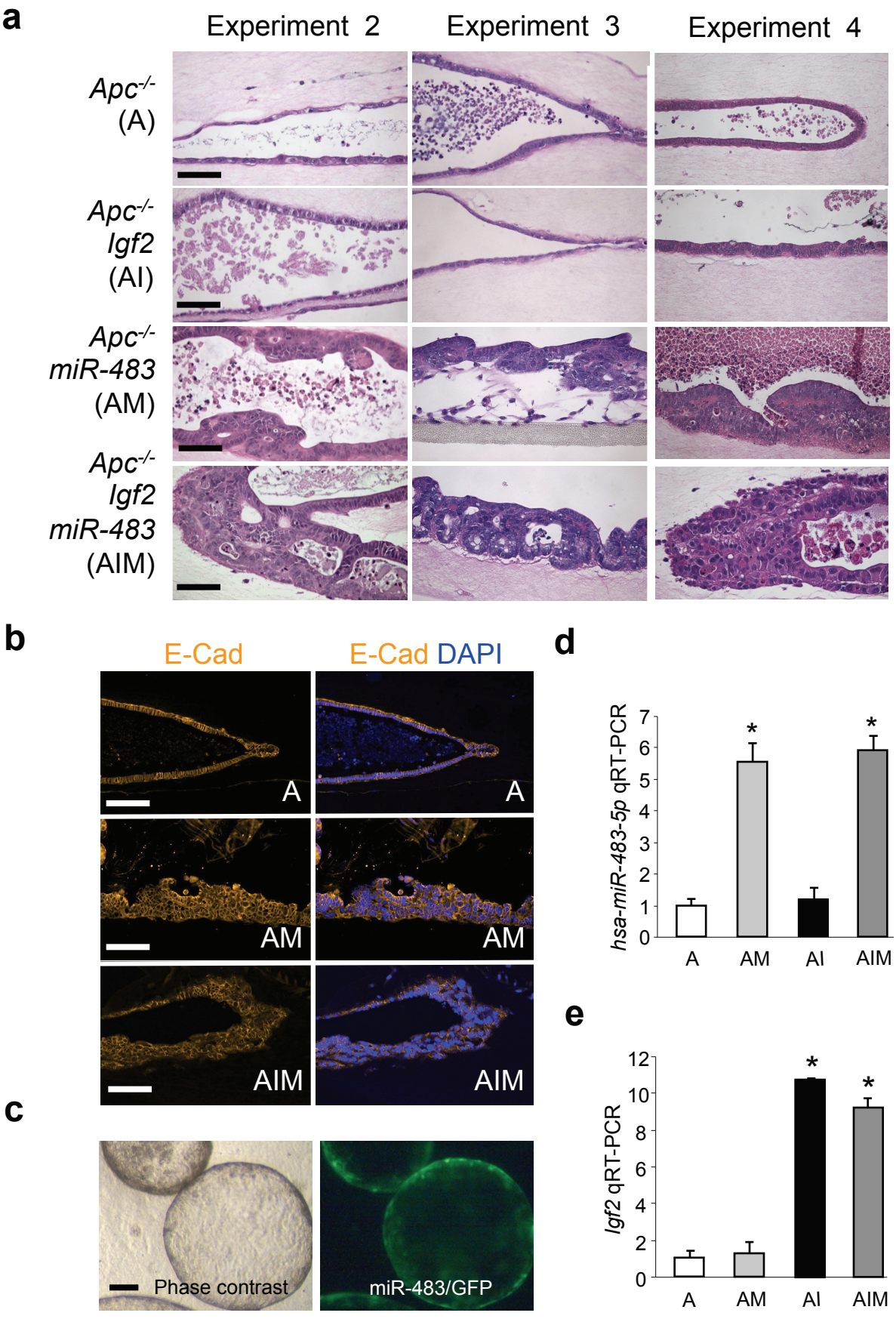

Supplementary Figure 9. Additional characterization of *miR-483* and *Igf2* gene manipulation in primary colon organoids.

(a) Additional biological replicates of Apc-null ("A") versus AI, AM, and AIM colon organoids. All images are culture day 50 after retroviral infection. Each image indicates a representative region from an individual experiment.

(b) *MiR-483*-containing modules AM and AIM induce epithelial dysplasia in adult colon organoids, day 50, E-cadherin immunofluorescence.

(c) Infection of *Apc*-null colon organoids by *miR-483/GFP* lentivirus. Fluorescence microscopy at 7-10 days post-infection revealed re-formation of organoids containing epithelial GFP signal.

(d, e). (d) *hsa-miR-483-5p* and (e) *Igf2* qRT-PCR in *Apc*-null colon organoids infected by *miR-483/GFP* lentivirus. FACS sorting was performed on *Apc*-null colon organoids at 14 days post-infection with *miR-483/GFP* and/or *Igf2-IRES-GFP* viruses to isolate RNA from EpCAM $^{+}$GFP^{+} cells (i.e. transduced colon epithelium) followed by stem-loop qRT-PCR for *hsa-miR-483-5p* or qRT-PCR for *Igf2*. Note appropriate overexpression of *miR-483* and/or *Igf2*. Also, *miR-483* overexpression did not significantly alter *Igf2* expression and vice-versa. n=3, Mean +/- SE. P value: *: $P < 0.01$

Supplementary Figure 10

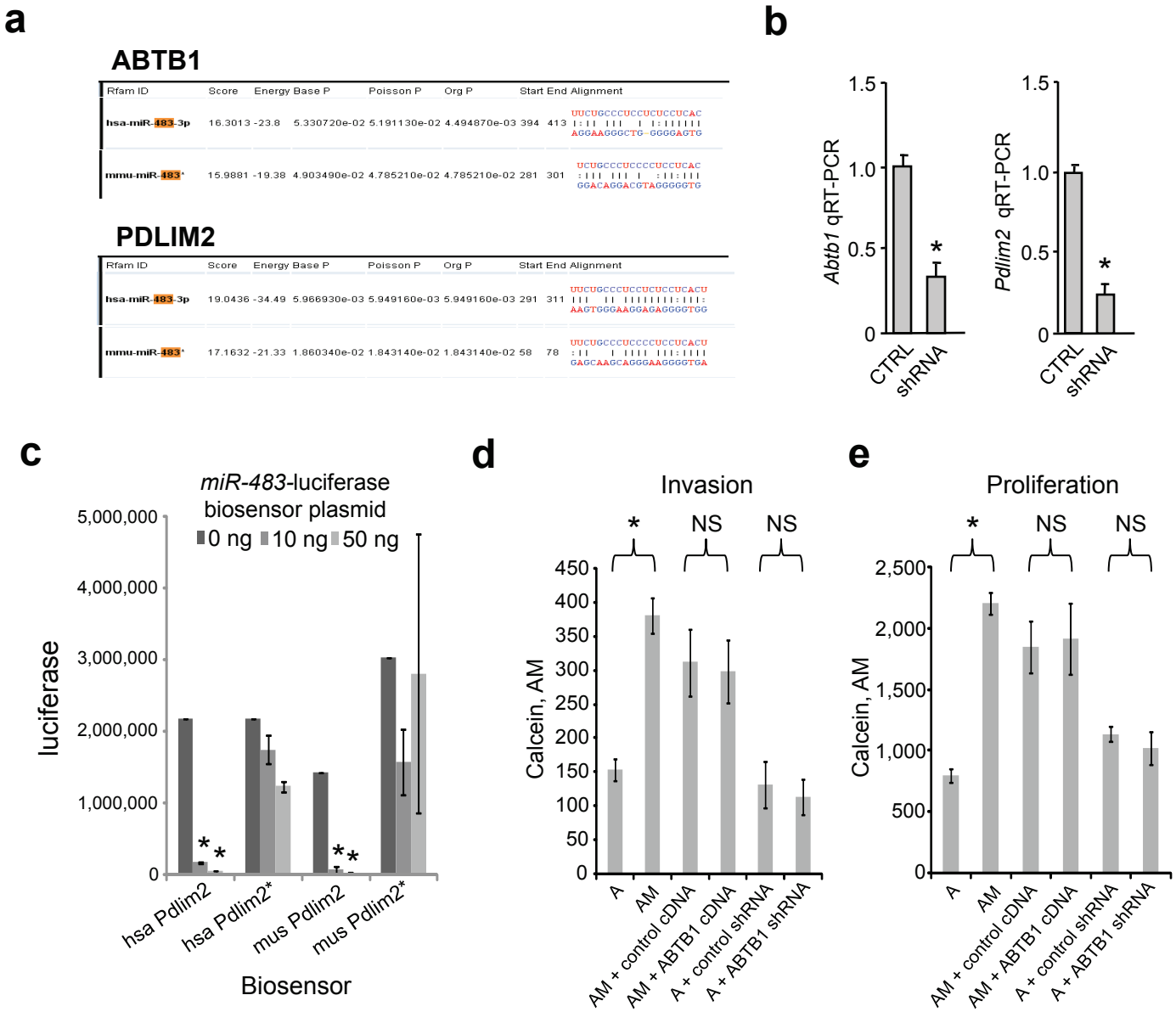

Supplementary Figure 10. *miR-483* suppression of *Abtb1* and *Pdlim2*.

(a) *Abtb1* and *Pdlim2* exhibit significant inverse correlation with *miR-483* amplification by analysis of colorectal patient data (COAD) from The Cancer Genome Atlas (TCGA) and MicroCosm. Sequences of human (Hsa) and mouse (Mmu) *miR-483* and corresponding 3' UTR binding sites for *Mmu/Hsa-miR-483* are conserved in *Abtb1* and *Pdlim2*.

(b) Validation of Abtb1 and Pdlim2 suppression by miR-483. *Abtb1* and *Pdlim2* RNA from HEK293T cells 5 days after infection with lentivirus encoding ABTB1 or PDLIM2 shRNA or negative control shRNA. n=3 experiments, mean +/- SE, * = P<0.05.

(c) Biosensor assay. *MiR-483* represses 3' UTR-luciferase reporters with wild type (mus Pdlim2 and hsa Pdlim2) but not mutant (mus Pdlim2* and hsa Pdlim2*) *miR-483* binding sites. Renilla luciferase was normalized to firefly luciferase. 0 ng, 10 ng and 50 ng of *miR-483* expression plasmid were transfected into 293T cells. n=4, mean +/- SE. *= P < 0.05.

(d) ABTB1 does not mediate *miR-483*-dependent invasion and proliferation. AM vs A modules were assayed for invasion and proliferation with lentiviral delivery of ABTB1 overexpression or shRNA knockdown.

Supplementary Figure 11

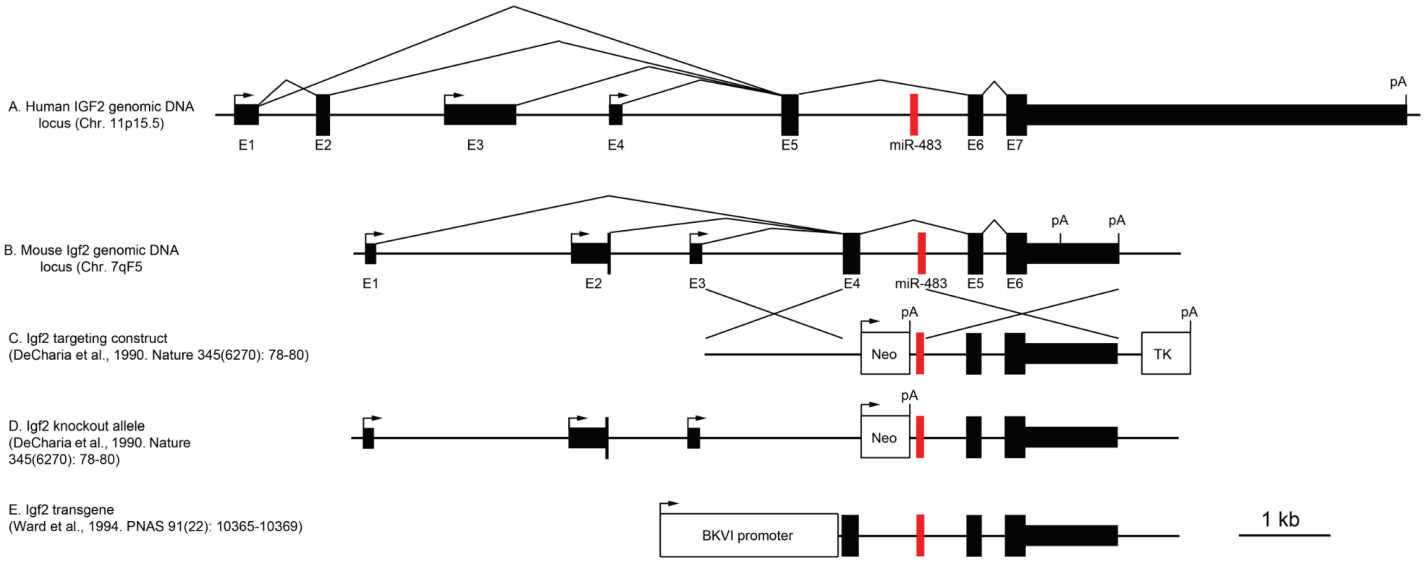

Supplementary Figure 11. Spatial relationship between *Igf2* and *miR-483* (red rectangle) within *Igf2* intronic sequences and previously described *Igf2* knockout and transgenic overexpressing cassettes.

(a) Organization of the human *IGF2* genomic locus on 11p15.5 with intronic *miR-483.*
(b) Organization of the mouse *Igf2* genomic locus on 7p with *miR-483* in intron 4.
(c, d) Schematic of the *Igf2* targeting construct (c) and recombined locus (d) used to generate an *Igf2* ko mouse (De Charia et al., 1990, Nature 345(6270): 78-80) that was used to determine effects on *Apc*-mediated tumorigenesis (Hassan et al., Cancer Res. 60, 1070-1076 (2000)). Note the presence of a *NeoR*/polyA cassette upstream of *miR-483* in mouse intron 4.
(e) Schematic of the *Igf2* transgenic construct used to generate an *Igf2* overexpressing mouse (Ward et al., PNAS 91(22): 10365-10369) that was used to determine synergy with *Apc*-mediated tumorigenesis (Hassan et al., Cancer Res. 60, 1070-1076 (2000)). The insert is an *Igf2* minigene containing intronic *miR-483* in mouse intron 4.

SUPPLEMENTARY DISCUSSION

Interestingly, prior studies demonstrating *Igf2*/*Apc* cooperation during murine polyposis[1] utilized a transgenic *Igf2* minigene containing *miR-483* in intron 4. Conversely, *Igf2* knockout mice used for *Apc* cooperativity studies contained neoR/polyA cassettes upstream of *miR-483* that likely disrupt *miR-483* expression[2,3] (**Supplementary Fig. 11)**. The alteration of *miR-483* expression in *Igf2* knockout mice has also been predicted by bioinformatic analysis of mouse knockouts of genes with intronic miRNAs[4]. A floxed *Igf2* allele that cooperates with *p53* loss deletes *Igf2* exons 4-6 including *miR-483*[5]. This intimate relationship between *Igf2* and *miR-483* may illustrate a general principle of inadvertent miRNA manipulation in knockout/transgenic mice[4], analogous to angiogenic phenotypes of the *Egfl7* locus being in fact attributable to *miR-126* contained within *Egfl7* intron 7[6]. Further, the possible contribution of intronic *miR-483* to *Igf2* locus imprinting-based effects on CRC[7] merits investigation, as suggested by *miR-483/Igf2* cooperation in organoid culture.

The pro-apoptotic gene *Puma/Bbc3,* and additional CRC tumor suppressor genes *Smad4 and Socs3* have been suggested to mediate *miR-483*-dependent effects in HCT116 cells, pancreatic and hepatocellular carcinoma cell lines respectively[8-11]. However, since in contrast to *PDLIM2* these targets are not repressed in *miR-483*-amplified cancers in the TCGA COAD/READ datasets, *PDLIM2* appears a more plausible *miR-483* target for human CRC. Furthermore *PDLIM2* undergoes homozygous deletion in human CRC (6% frequency; www.cbioportal.org[12]) and is hypermethylated in CRC cell lines[13].

1. Hassan, A.B. & Howell, J.A. Insulin-like growth factor II supply modifies growth of intestinal adenoma in Apc(Min/+) mice. *Cancer Res* **60**, 1070-1076 (2000).
2. Ward, A., Bates, P., Fisher, R., Richardson, L. & Graham, C.F. Disproportionate growth in mice with Igf-2 transgenes. *Proc Natl Acad Sci U S A* **91**, 10365-10369 (1994).
3. DeChiara, T.M., Efstratiadis, A. & Robertson, E.J. A growth-deficiency phenotype in heterozygous mice carrying an insulin-like growth factor II gene disrupted by targeting. *Nature* **345**, 78-80 (1990).

4. Osokine, I., Hsu, R., Loeb, G.B. & McManus, M.T. Unintentional miRNA ablation is a risk factor in gene knockout studies: a short report. *PLoS Genet* **4**, e34 (2008).
5. Haley, V.L.*, et al.* Igf2 pathway dependency of the Trp53 developmental and tumour phenotypes. *EMBO Mol Med* **4**, 705-718 (2012).
6. Kuhnert, F.*, et al.* Attribution of vascular phenotypes of the murine Egfl7 locus to the microRNA miR-126. *Development* **135**, 3989-3993 (2008).
7. Timp, W., Levchenko, A. & Feinberg, A.P. A new link between epigenetic progenitor lesions in cancer and the dynamics of signal transduction. *Cell Cycle* **8**, 383-390 (2009).
8. Veronese, A.*, et al.* Oncogenic role of miR-483-3p at the IGF2/483 locus. *Cancer Res* **70**, 3140-3149 (2010).
9. Hao, J., Zhang, S., Zhou, Y., Hu, X. & Shao, C. MicroRNA 483-3p suppresses the expression of DPC4/Smad4 in pancreatic cancer. *FEBS Lett* **585**, 207-213 (2011).
10. Ma, N.*, et al.* Igf2-derived intronic miR-483 promotes mouse hepatocellular carcinoma cell proliferation. *Mol Cell Biochem* **361**, 337-343 (2012).
11. Rigby, R.J., Simmons, J.G., Greenhalgh, C.J., Alexander, W.S. & Lund, P.K. Suppressor of cytokine signaling 3 (SOCS3) limits damage-induced crypt hyper-proliferation and inflammation-associated tumorigenesis in the colon. *Oncogene* **26**, 4833-4841 (2007).
12. Cerami, E.*, et al.* The cBio cancer genomics portal: an open platform for exploring multidimensional cancer genomics data. *Cancer Discov* **2**, 401-404 (2012).
13. Qu, Z.*, et al.* DNA methylation-dependent repression of PDZ-LIM domain-containing protein 2 in colon cancer and its role as a potential therapeutic target. *Cancer Res* **70**, 1766-1772 (2010).